

Naval Research Laboratory

Washington, DC 20375-5320



NRL/MR/6755--01-8571

The Effect of Electric Field Structure on Joule Heating II: An Expanded Data Set

DAVID N. WALKER
WILLIAM E. AMATUCCI

*Charged Particle Physics Branch
Plasma Physics Division*

GURUDAS I. GANGULI
*Beam Physics Branch
Plasma Physics Division*

September 28, 2001

Approved for public release; distribution is unlimited.

20011010 055

REPORT DOCUMENTATION PAGE

Form Approved
OMB No. 0704-0188

Public reporting burden for this collection of information is estimated to average 1 hour per response, including the time for reviewing instructions, searching existing data sources, gathering and maintaining the data needed, and completing and reviewing this collection of information. Send comments regarding this burden estimate or any other aspect of this collection of information, including suggestions for reducing this burden to Department of Defense, Washington Headquarters Services, Directorate for Information Operations and Reports (0704-0188), 1215 Jefferson Davis Highway, Suite 1204, Arlington, VA 22202-4302. Respondents should be aware that notwithstanding any other provision of law, no person shall be subject to any penalty for failing to comply with a collection of information if it does not display a currently valid OMB control number. **PLEASE DO NOT RETURN YOUR FORM TO THE ABOVE ADDRESS.**

1. REPORT DATE (DD-MM-YYYY) September 28, 2001			2. REPORT TYPE Interim Report		3. DATES COVERED (From - To)	
4. TITLE AND SUBTITLE The Effect of Electric Field Structure on Joule Heating II: An Expanded Data Set					5a. CONTRACT NUMBER	
					5b. GRANT NUMBER	
					5c. PROGRAM ELEMENT NUMBER	
6. AUTHOR(S) David N. Walker, William E. Amatucci, and Gurudas I. Ganguli					5d. PROJECT NUMBER	
					5e. TASK NUMBER	
					5f. WORK UNIT NUMBER	
7. PERFORMING ORGANIZATION NAME(S) AND ADDRESS(ES) Naval Research Laboratory Washington, DC 20375-5320					8. PERFORMING ORGANIZATION REPORT NUMBER NRL/MR/6755--01-8571	
9. SPONSORING / MONITORING AGENCY NAME(S) AND ADDRESS(ES) Office of Naval Research 800 North Quincy Street Arlington, VA 22217					10. SPONSOR / MONITOR'S ACRONYM(S)	
					11. SPONSOR / MONITOR'S REPORT NUMBER(S)	
12. DISTRIBUTION / AVAILABILITY STATEMENT Approved for public release; distribution is unlimited.						
13. SUPPLEMENTARY NOTES						
14. ABSTRACT Emissive probe and ion energy analyzer diagnostics have been used to deduce the effect of electric field scale size on ion temperature in space simulation of ion heating in a large vacuum chamber. Results suggest an increase in ion temperature as a function of electric field scale size but a limit proportional to mean free path.						
15. SUBJECT TERMS Ion heating, Electric field						
16. SECURITY CLASSIFICATION OF:			17. LIMITATION OF ABSTRACT	18. NUMBER OF PAGES	19a. NAME OF RESPONSIBLE PERSON	
a. REPORT	b. ABSTRACT	c. THIS PAGE			David Walker	
Unclassified	Unclassified	Unclassified	UL	14	19b. TELEPHONE NUMBER (include area code) 202-767-2248	

The effect of electric field structure on Joule heating II: An expanded data set

David N. Walker¹, William E. Amatucci¹, and Gurudas I. Ganguli²

¹Charged Particle Physics Branch

²Beam Physics Branch

Plasma Physics Division

Naval Research Laboratory

Washington, DC

Abstract

In an earlier work we described an experimental series which demonstrates ion Joule heating in the presence of a potential profile with a single peak. As a part of this effort we demonstrated the ability to control the magnitude and direction of the electric field (or the sign of potential change) in space in a simulated ionospheric environment. We demonstrated that we are able to produce ion heating in this environment as a function of ion-neutral collision frequency consistent with the calculated Joule heating rate. Our ultimate aim is to fully characterize the effect of electric field structure on the heating by varying the localization of the fields (e.g., creating multiply-peaked potential distributions, varying the scale size of the field) and by allowing the potentials to have a time-dependent amplitude. In space, this implies multiple localized structuring and in time it implies a frequency variation from the ELF range to the ion plasma frequency. In results presented here, we have increased the data sample and varied the spatial size of the fields only. In a few instances we have produced doubly-peaked potential profiles. Consistent with earlier results, we have been able to demonstrate a peak in the ion temperature as a function of collision frequency. **New results shown in this data indicate that for approximately constant pressure and electric field, the normalized ion temperature increases with the scale size of the electric field region but the data suggests a limit to this increase (for a given scale size) which is proportional to the mean free path for ion neutral collisions, λ_{in} .** We base this conclusion on using the frequency-width-at-half-maximum (fwhm) of the electric field region as a marker of the spatial scale size which we designate as L_E . In addition to this,

Introduction

Perhaps the most spectacular example of a natural phenomenon influenced by small scale plasma structuring is an auroral display. Auroral arcs are often quite thin [Borovsky, 1993] and the observed development of curls gives indications of steep gradients in electron flux and other plasma parameters. More generally, irregularities which develop in ionospheric plasma density, currents, and electric fields have been studied for a number of years using both ground-based and *in situ* plasma diagnostics [Sofko and Huang, 2000; Christensen et al., 1997; Fejer and Kelley, 1980; Schlegel and Neilsen, 1985]. Irregular structure is evident in all regions of the ionosphere from the auroral to equatorial zones and is observed to vary from scales as small as meters to as large as

kilometers [Kelly and Carlson, 1977; Mozer et al., 1977; Basu et al., 1988; Tsunoda et al., 1989; Holmgren and Kintner, 1990]. However, unambiguous resolution of small scale structures, whose characteristics may also be a function of time, and their effect on other plasma parameters, is often difficult to claim from a moving space vehicle. There is the widely known space-time ambiguity to be addressed in these measurements and, therefore, often a comparison to theory is not very convincing. Our laboratory investigation is designed to determine the dependence of Joule heating on electric field variability in a controlled environment. These laboratory experiments which are performed under controlled, reproducible plasma conditions are scaled to those in the ionosphere and can help can provide insight by effectively decoupling space and time and elucidating the important underlying physics [Rynn and D'Angelo, 1960; Motley, 1975; Amatucci et al., 1996; Gekelman et al., 1997; Walker et al., 1997, 2001].

Localized electric fields in the laboratory are produced by a set of concentric, separately biased, conducting rings which are aligned axially along a large cylindrical vacuum chamber. The experimental facility, including the plasma characterization, diagnostic instrumentation and the arrangement of the electric field-producing rings, is described in much of our earlier work, eg., [Amatucci et al., 1996]. For further introduction to the experiments described here and their relevance to space physics issues we refer the interested reader to either the first NRL Memorandum Report on this work of Walker et al., [2000] or to Walker et al., [2001]. Our intention with the current work is to generate a broad data base of the effects of electric field structure on Joule heating by varying both the space, time and directional characteristics of the electric fields themselves and measuring the resulting heating. The parameter space which we cover includes the magnetic field, neutral density, electric field magnitude, scale length, and, in future efforts, time variation of the electric field magnitude. This interim report provides results to date.

Range of electric field variation

Shown in Figure 1 is a plot of the maximum electric field measured in a number of independent runs versus the full-width-at-half-maximum (fwhm) of the electric field region. Measurements of plasma potential were made during radial traversals of an emissive probe at a fixed axial position (z) approximately 30 cm along z from the rings as described in Walker et al., [2000,2001]. The electric field is determined by differentiating these profiles with respect to r and then characterizing the region over which they act by the fwhm (which we later designate as L_E , the scale size of the region). An example of a particular single-peaked profile and its electric field is shown in Figures 2 and 3. In Figure 2 we show the potential profile and a fit to the profile (dashed line); In Figure 3 we show the 1st derivative of the fitted profile and, as a dashed line, the 2nd derivative. Indicated in the Figure 3 is an approximation to the fwhm.

Figure 1 is made without regard to neutral pressure which varies over almost two orders of magnitude from 10^{-3} to 10^{-5} Torr. This plot therefore is useful only as an indication of the range of electric fields and scale lengths investigated in the initial experimental series. As seen in the figure, the range of the electric field varies from a maximum of 11 volts/cm to a minimum of less than a volt/cm, while the scale size of the region, L_E , can vary from less than 4 cm to near 9 cm. This reasonably wide variability can be used to provide the basis of plasma structure variation effects

through localization.

Examples of multiply-peaked potential profiles

Figures 4 and 5 are examples of ion temperature measurements taken in a radial sweep across the chamber when the potential distribution has two peaks. Figure 4 is a plot of the potential distribution versus radius and Figure 5 is the resulting measured normalized ion temperature. The ion temperature is normalized to the background value far away from the electric field region. These measurements were taken for a neutral pressure of 3×10^{-4} Torr and a magnetic field of 40 gauss along the z-axis. As in our earlier work, the correlation of the incidence of increased ion heating with electric field structure is evident. Since ionospheric Joule heating processes are thought to occur through structures which vary in time and/or space such as these, it is important to investigate a variety of features associated with multiple structures.

Although the profiles presented show only small excursions in potential they are nevertheless representative of the range of variation possible with the multiple rings in the chamber. We conclude from the data in subsequent sections that ion temperature is dependent on the scale size of the structure, i.e., even for regions with the same total potential drop (which can roughly be approximated as $E_{\max}L_E$) the scale size of the region is important in determining the ultimate ion temperature. In addition to this, the data suggest a limit to the ion heating based on a comparison of the acceleration region size to the mean free path for ion neutral collisions. Below we concentrate on the effect of the scale size considering first only a single-peaked potential profile.

Dependence of ion temperature on electric field localization

Once having established that we are able to vary the spatial extent of the field profile (i.e., vary the field localization in space) as shown above, we are able to test effects on ion temperature. Shown in Figure 6 is a plot of T_i versus $E_{\max}L_E$ for all magnetic fields used (10g, 30g, 40g, 50g) and neutral pressures. We have restricted the data to the range such that $E_{\max}L_E$ (or the change in potential) is less than 10 volts. What we wish to emphasize in presenting the data in this manner is the T_i dependence not only on the total potential drop, $E_{\max}L_E$, but also on neutral pressure and the size of the acceleration region, i.e., neutral pressure and the size of the acceleration region contribute to the large spread in the data shown.

To isolate partly the effects of neutral pressure Figures 7 through 9 are an indication of the effect on T_i of varying the size of the electric field region. Each data set is accompanied by a linear fit simply to indicate the trend. Each plot is of normalized (maximum) ion temperature versus the scale size of the electric field region. The ion temperature, normalized by the background value, refers to the maximum temperature attained during a radial traversal of the ion energy analyzer across the vacuum chamber. All plots are chosen for a potential drop between about 1 and 2 volts or, $1 < E_{\max}L_E < 2$ volts, where again L_E represents the size of the electric field (fwhm, as described above) and E_{\max} is the maximum value of that field. In Figure 7 the neutral pressure is

approximately constant at $P_N = 7.5 \times 10^4$ Torr and an electric field magnitude is chosen in the range $0.5 < E_{\max} < 1$ volts/cm. By contrast Figure 8 is data taken at the same pressure but for a smaller electric field. In this case we have chosen $0 < E_{\max} < 0.35$ volts cm^{-1} to select lower electric fields and also for the practical matter that many of the measured fields fall in this range. There are two things to notice when comparing these two figures. First, the ion temperature for the same electric field region scale size is higher for the higher electric field case of Figure 7. Also, the general slope as indicated by the straight lines is larger for the higher electric field case. Figure 9 is another data set where, in this case, the range of electric fields chosen is the same as in Figure 1 above, $0.0 < E_{\max} < 0.35$ volts/cm, but the neutral pressure is chosen to be larger, $10^{-3} < P_N < 3 \times 10^{-3}$, to observe its effect on temperature. One notices that the temperatures are again lower at the same scale sizes for the case of higher neutral pressure in Figure 9 versus that of Figure 8. This observation is cited in the next section in the context of the effect of increasing ion neutral collisions on the ability of the ions to respond to the electric field. These preliminary results seem to bear out, at least for these pressure ranges, what one intuitively expects, i.e., the greater the spatial extent of an electric field region to which an ion is exposed in transit, the greater the increase in temperature produced and the larger the applied field the greater the temperature increase for the same scale size.

Summary plot of ion temperature vs. pressure

Figure 10 is a summary plot of the effect of neutral pressure on T_i . The plot was made by again restricting as above the electric field to $0 < E_{\max} < 0.35$ volts/cm and the range of $E_{\max} L_E$ to between 1 and 2 volts. The plot shows the average ion temperature at a number of pressures. The error bars on the data are the standard deviations of the measured temperature sets at each pressure. The rather large standard deviations evident in the two pressure ranges near maximum T_i are the result of the fact that those data sets each have the most data and they have wider ranges of L_E than the other data sets. The data is in fact rather sparse in the other data sets containing typically 3 points only due to the boundary conditions above on $E_{\max} L_E$. It was shown in earlier work [Walker et al., 2001] that ion temperature tends to reach a maximum at the peak of the Joule heating rate curve which is strongly dependent on the Pedersen conductivity and therefore ion-neutral collision frequency (or neutral pressure). In the present case, the results shown are for a plasma density of $5 \times 10^7 \text{ cm}^{-3}$ and a magnetic field of 40 gauss. In that case the Pedersen conductivity peaks at a pressure slightly smaller than 10^{-3} Torr. Figure 10 shows the steep drop off in temperature beyond 10^{-3} Torr and it also reaches a maximum just before this at about 8×10^{-4} Torr; very near the pressure at Pedersen conductivity maximum. Also, moving to smaller pressures from the maximum temperature, the temperature falls fairly dramatically until at 5×10^{-4} Torr it is half its value at maximum. As neutral pressure tends toward very low levels, we expect there to be essentially no contribution to ion heating from collisions [Amatucci et al., 1999].

Collisions and a natural limit to the increase in T_i ?

At a pressure near 10^{-3} Torr (which is where the majority of the data was taken) the mean free path for collisions of argon ions with neutrals, λ_{in} , is on the order of the ion gyroradius, ρ_i , at a magnetic field of 40 gauss as shown in the plot of Figure 11 where we plot λ_{in} normalized by ρ_i , as

a function of pressure. As we move to pressures much less than 10^{-3} Torr, λ_{in} is quite large compared to ρ_i so that magnetic field effects become increasingly important as one moves toward lower pressure. The actual size of λ_{in} is shown in Figure 12 and we note that it varies from about 3 cm at 10^{-3} Torr to about 30 cm at 10^{-4} Torr and is seen to be comparable to the range of L_E from the experimental data shown in Figure 1. Keeping in mind that fwhm (or L_E) is really about half the acceleration region size, we can see that at pressures between 10^{-3} and 10^{-4} Torr, λ_{in} is comparable to the size of L_E . Also, the ion neutral collision frequency shown in Figure 13 for the same magnetic field is approximately the same as the ion gyrofrequency at 10^{-3} torr. For these pressures then and those greater than this, the ions, while not able to complete coherent orbits, can likely not even experience the full potential drop since they are hindered in this motion by the frequency of these collisions; consequently there should be a drop off in ion temperature as a function of pressure and this is in fact observed above in Figure 10. However, recall that Figure 10 is plotted for a range of L_E . As we have demonstrated above in Figures 7 through 9 there is generally an increase in ion temperature consistent with an increase in the size of L_E . However, in the data of Figure 8 (pressure of 7.5×10^{-4} Torr with $\lambda_{in} = 3.5$ cm) and Figure 9 (pressure range of $10^{-3} < P_n < 3 \times 10^{-3}$ Torr and λ_{in} in the range $0.87 < \lambda_{in} < 2.6$ cm), we observe what could be a peak in the data beyond an L_E of about 6.2 cm in Figure 9 and between 7 and 8 cm in Figure 8. This is consistent with the idea of a limit occurring at lower scale sizes for higher pressures where this limit is related to λ_{in} . These are the highest pressure ranges for this data set and could be an indication of natural limit to the magnitude of T_i when looking for heating in structured electric fields. This behavior is being investigated in present work.

Conclusions

We have increased the size of our data sample and have begun an investigation of the effect of electric field structure on ion heating. Our data suggest that ion temperature generally increases with increasing scale size of the electric field region but tends to maximize probably as a function of the relative scale size of the acceleration region to the mean free path for ion neutral collisions. Our data shows a peak in the measured ion temperature as a function of neutral pressure generally consistent with the pressure region of maximum Pedersen conductivity, although somewhat larger.

Acknowledgments

This work was supported by the Office of Naval Research (ONR)

References:

- Amatucci, W.E., G. Ganguli, D.N. Walker, J.A. Antoniadis, D. Duncan, J.H. Bowles, V. Gavrishchaka, and M.E. Koepke, Plasma Response to strongly sheared flow, *Phys. Rev. Lett.*, *77*, 1978, 1996
- Basu, S., S. Basu, E. Mackenzie, P.F. Fougere, W.R. Colley, N. C. Maynard, J.D. Winningham, M. Sugiura, W.B. Hanson, and W.R. Hoegy, Simultaneous density and electric field fluctuation spectra associated with velocity shears in the auroral oval, *J. Geophys. Res.*, *93*, 115, 1988
- Borovsky, J.E., Auroral arc thicknesses as predicted by various theories, *J. Geophys. Res.*, *98*, 6101, 1993
- Christensen, A.B., J.H. Hecht, R.L. Walterscheid, M.F. Larsen and W.E. Sharp, Depletion of oxygen in aurora: Evidence for a local mechanism, *J. Geophys. Res.*, *102*, 22,273, 1997
- Fejer, B.G. and M.C. Kelley, Ionospheric irregularities, *Rev. Geophys.*, *18*, 401, 1980
- Gekelman, W., S. Vincena, D. Leneman, and J. Maggs, Laboratory experiments on shear Alfvén waves and their relationship to space plasma, *J. Geophys. Res.*, *102*, 7225, 1997
- Holmgren, G., and P.M. Kintner, Experimental evidence of widespread regions of small-scale plasma irregularities in the magnetosphere, *J. Geophys. Res.*, *95*, 6015, 1990
- Kelley, M.C., and C.W. Carlson, Observation of intense velocity shear and associated electrostatic waves near an auroral arc, *J. Geophys. Res.*, *82*, 2343, 1977
- Motley, R.W., *Q Machines*, Academic, San Diego, CA, 1975
- Rynn, N., and N. D'Angelo, Device for generating a low temperature, highly ionized cesium plasma, *Rev. Sci. Instrum.*, *31*, 1326, 1960
- Schlegel, K., and E. Nielsen, Foreword: Irregularities in the high latitude ionosphere, *Radio Sci.*, *20*, 675, 1985
- Sofko, G.J. and C-S Huang, SuperDARN observations of medium-scale gravity wave pairs generated by Joule heating in the auroral zone, *Geophys. Res. Lett.*, *27*, 485, 2000
- Tsunoda, R.T., R.C. Livingston, J.F. Vickrey, R.A. Heelis, W.B. Hanson, F.J. Rich, and P.F. Bythrow, Dayside observations of thermal ion upwellings at 800-km altitude: An ionospheric signature of the cleft ion fountain, *J. Geophys. Res.*, *94*, 15,277, 1989

Walker, D.N., W.E. Amatucci, G. Ganguli, *The Effect of Electric Field Structure on Joule Heating*,
NRL Memorandum Report NRL/MR/6750-00-8449, 2000

Walker, D.N., W.E. Amatucci, G. Ganguli, J.A. Antoniadis, J.H. Bowles and D. Duncan,
Perpendicular ion heating by velocity-shear-driven waves, *Geophys. Res. Lett.*, 1187, 1997

Walker, D.N., W.E. Amatucci, G. Ganguli, Characterization of Joule heating in structured electric
field environments, *J. Geophys. Res.*, 106, 1807, 2001

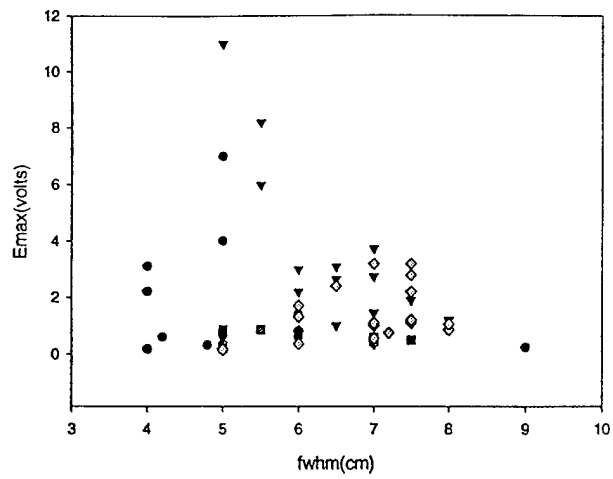


Figure 1

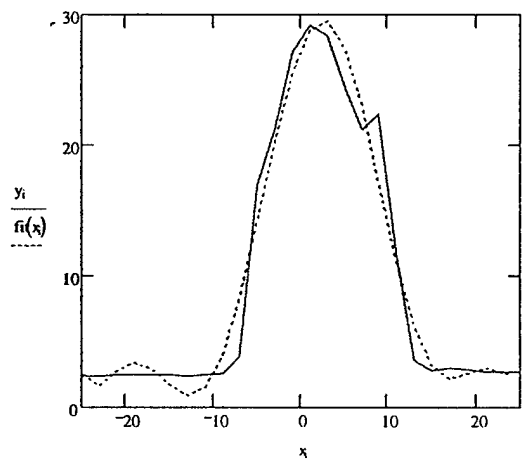


Figure 2

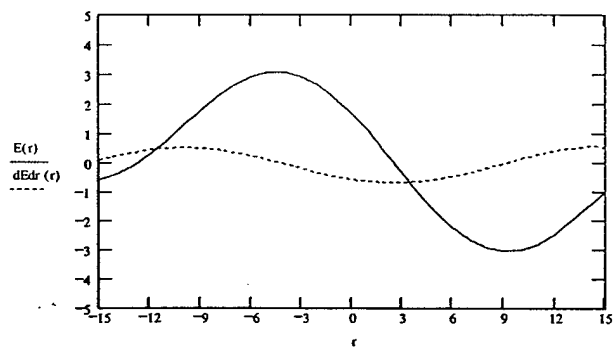


Figure 3

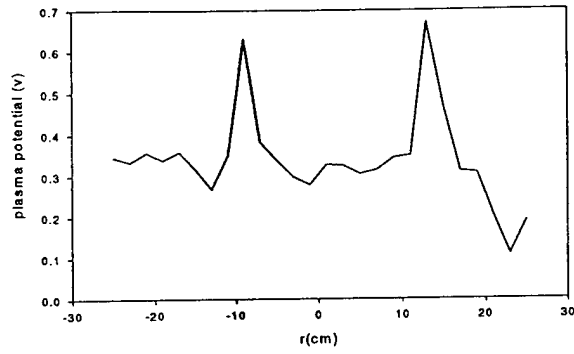


Figure 4

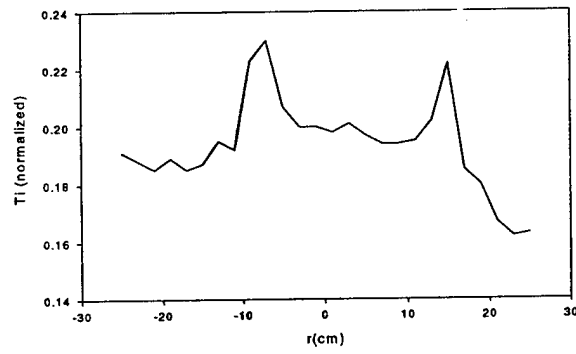


Figure 5

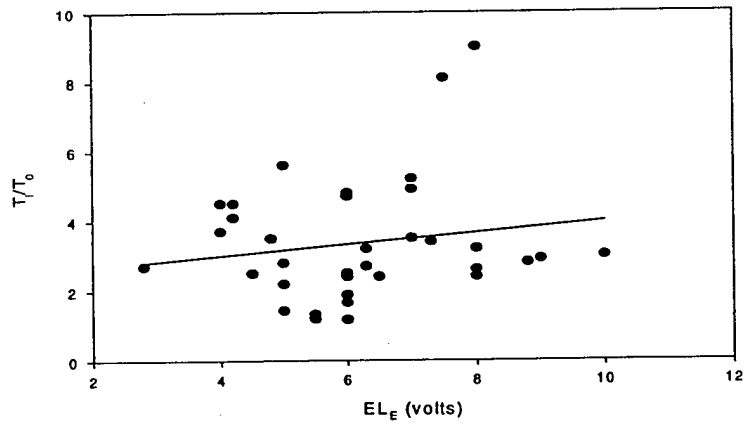


Figure 6

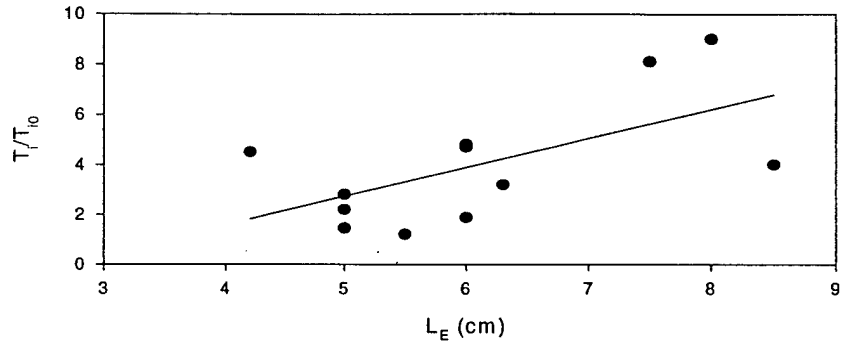


Figure 7

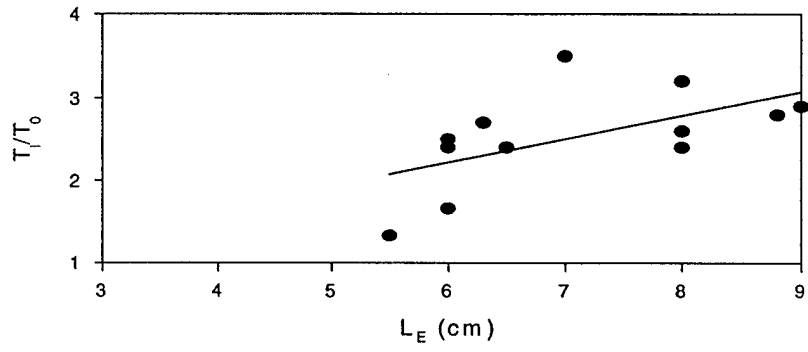


Figure 8

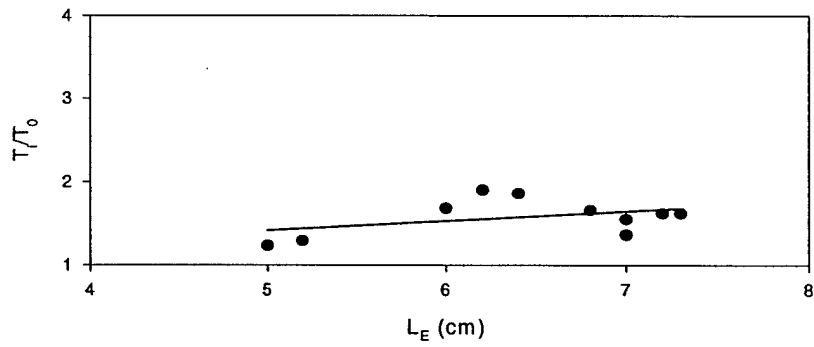


Figure 9

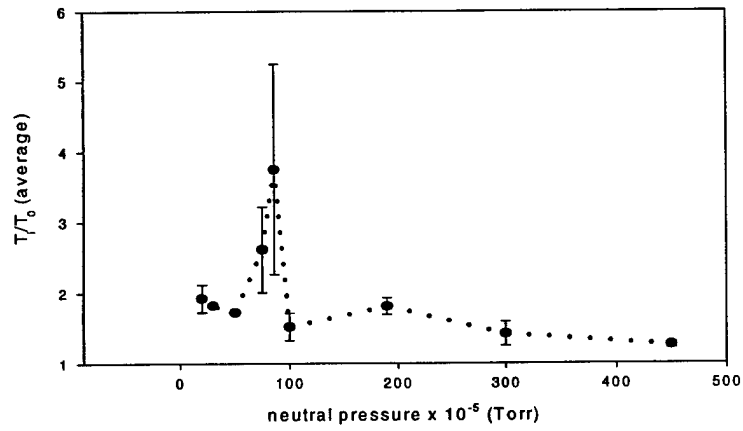


Figure 10

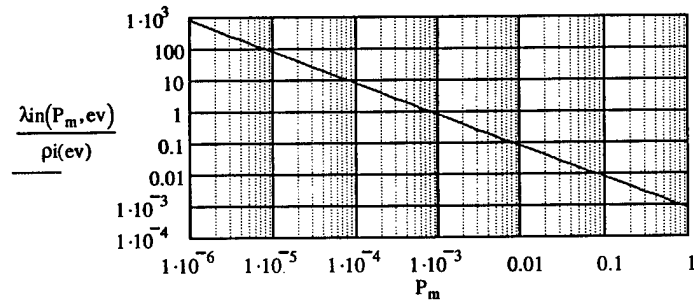


Figure 11

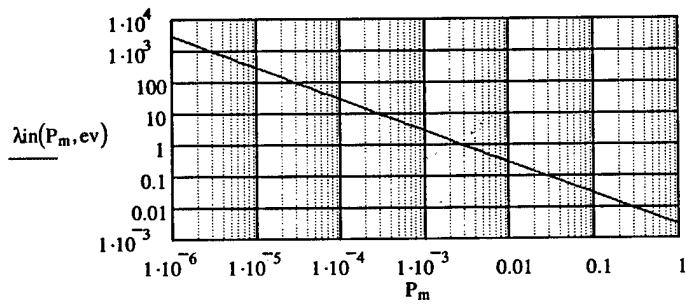


Figure 12

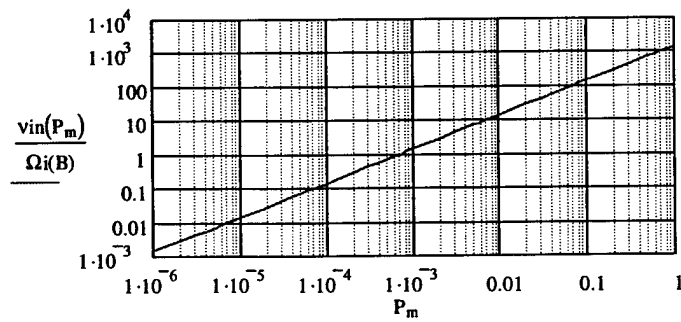


Figure 13